ARTICLE

Deep Euteceic Solvents-assisted Synthesis of Novel Network Nanostructures for Accelerating Formic Acid Electrooxidation

Jun-Ming Zhang [a,b,c,*], Xiao-Jie Zhang [a,b], Yao Chen [a], Ying-Jian Fang [a], You-Jun Fan [b,*], Jian-Feng Jia [a,*]

[a] Key Laboratory of Magnetic Molecules & Magnetic Information Materials Ministry of Education, The School of Chemical and Material Science, Shanxi Normal University, Taiyuan, 030031, Shanxi, China
[b] Guangxi Key Laboratory of Low Carbon Energy Materials, College of Chemistry and Pharmaceutical Sciences, Guangxi Normal University, Guangxi, Guilin, 541004, China
[c] Kunshan Superior Silk Screen Printing Material Co., LTD, Kunshan, 215300, Jiangsu, China

Abstract

Deep eutectic solvents (DESs) have been reported as a type of solvent for the controllable synthesis of metal nanostructures. Interestingly, flower-like palladium (Pd) nanoparticles composed of staggered nanosheets and nanospheres are spontaneously transformed into three-dimensional (3D) network nanostructures in choline chloride-urea DESs using ascorbic acid as a reducing agent. Systematic studies have been carried out to explore the formation mechanism, in which DESs itself acts as a solvent and soft template for the formation of 3D flower-like network nanostructures (FNNs). The amounts of hexadecyl trimethyl ammonium bromide and sodium hydroxide also play a crucial role in the anisotropic growth and generation of Pd-FNNs. The low electrocatalytic performance of Pd is one of the major challenges hindering the commercial application of fuel cells. Whereas, the 3D Pd-FNNs with lower surface energy and abundant grain boundaries exhibited the enhanced electrocatalytic activity and stability toward formic acid oxidation, by which the mass activity and specific activity were 2.7 and 1.4 times higher than those of commercial Pd black catalyst, respectively. Therefore, the current strategy provides a feasible route for the synthesis of unique Pd-based nanostructures.

Keywords: Deep eutectic solvents; Palladium; Network nanostructure; Formic acid; Electro-oxidation

1. Introduction

Direct formic acid fuel cell (DFAFC), a subcategory of proton exchange membrane fuel cells, has the advantages of low acid penetration into Nafion membrane, higher energy density, and high theoretical open circuit potential, and is considered to be an ideal energy conversion device applied in portable electronic equipments [1–3]. Over the past few decades, a great deal of work has been devoted to the research and development of novel catalysts. Among the numerous 3 d transition metals, palladium (Pd) has been extensively studied in DFAFC because of its relatively abundant resources and better performance for formic acid oxidation [4–6]. Formic acid oxidation reaction (FAOR) can proceed through two different reaction mechanisms, that is, the dehydrogenation pathway and the dehydration pathway [7–9]. Most Pt-based catalysts electrocatalytically oxidize $HCOOH_{ads}$ molecules to CO_{ads} intermediate through the dehydration pathway, and then continue to oxidize CO to CO_2 at high potentials. Compared with Pt-based catalysts, Pd-based catalysts directly oxidize

Received 23 June 2022; Received in revised form 19 July 2022; Accepted 21 July 2023
Available online 21 July 2022

* Corresponding author, Jun-Ming Zhang, Tel: (86-351)2051192, E-mail address: zhangjunming@sxnu.edu.cn.
* Corresponding author, You-Jun Fan, Tel: (86-773)5846279, E-mail address: youjunfan@mailbox.gxnu.edu.cn.
* Corresponding author, Jian-Feng Jia, Tel: (86-351)2051192, E-mail address: jiajf@dns.sxnu.edu.cn.

https://doi.org/10.13208/j.electrochem.2206231

HCOOH molecules to CO_2 via the dehydrogenation pathway, avoiding the poisoning effect of CO species on the catalysts. However, the main challenge hindering the practical application of DFAFC remains the lack of highly active catalysts with low cost and long-term stability. Surface engineering is an effective strategy to reduce Pd loading and improve reactivity, such as regulating morphology, composition, structure, etc. [10−13].

The physical-chemical properties of nanomaterials are largely dependent on the morphology, so that the shape-controlled synthesis of metal nanostructure has become one of the hotspots in the field of scientific research [14−16]. The application performance in various fields, such as sensors, plasmonics, medicine, and fuel cells, is expected to be enhanced by the synthesis of special shapes [17]. Network nanostructures have attracted increasing attention because they can significantly improve electrocatalytic activity. Network nanostructures have the following advantages: more lively high-density atomic defects (such as steps, kinks, edges) are beneficial for electrocatalytic reactions; the unique structure in electrochemical reactions promotes the mass exchange and gas diffusion; the interconnected structure can suppress the dissolution and agglomeration of nanomaterials [18]. For example, Xu et al. successfully prepared 3D Pd polyhedron network structure by Cu^{2+}-assisted one-step solution-chemical method, which exhibited excellent electrocatalytic performance for formic acid oxidation [19]. AuPd nanowire networks were synthesized by co-reduction method using theophylline as a structure-directing agent, which provided an enlarged ECSA and a large number of active sites [20]. The literature reported the synthesis of network structures with various components in water, such as Pd polyhedron networks [19], Pd nanochain networks [21], $Ni_{0.75}Cu_{0.25}$ [22], and so on. Deep eutectic solvents (DESs) is a kind of special ion liquid analogs that can be obtained simply by thermally mixing quaternary ammonium salt and hydrogen bond donor. DESs with unique properties of low cost, non-toxicity, excellent ionic conductivity, good thermal stability, wide electrochemical stability window, and environmental friendliness, is more and more used as green solvents in various fields [23−25]. So far, the synthesis of Pd nanocrystals in DESs has been confined to the zero-dimensional nanoparticles, and there are few reports on the preparation of 3D Pd network nanostructures in DESs.

Herein, a kind of 3D flower-like Pd network nanostructures (Pd-FNNs) was successfully synthesized in choline chloride-urea DESs medium via a simple one-step solvothermal method. If the concentrations of the two reactants, NaOH and CTAB, are 0.3 $mmol \cdot L^{-1}$ and 0.0825 $mmol \cdot L^{-1}$, respectively, the Pd seeds will evolve into FNNs. X-ray diffraction (XRD), scanning electron microscopy (SEM), transmission electron microscopy (TEM) and X-ray photoelectron spectroscopy (XPS) were used to characterize the as-prepared nanostructures. Electrochemical methods were used to compare the electrocatalytic performance and anti-CO poison ability of Pd-FNNs, coral-like palladium network nanostructures (Pd-CNNs), Pd-Water, and commercial Pd black. The results showed that the Pd-FNNs possessed the enhanced FAOR electrocatalytic activity, and the mass activity and specific activity reached 1551.8 $mA \cdot mg_{Pd}^{-1}$ and 6.96 $mA \cdot cm^{-2}$, respectively. Furthermore, Pd-FNNs exhibited better resistance to CO poisoning and better stability compared with other catalysts. This work lays the foundation for the synthesis of other Pd-based nanostructures in DESs.

2. Experimental

2.1. Chemicals

Palladium chloride ($PdCl_2$), choline chloride, urea, ascorbic acid (AA), hexadecyl trimethyl ammonium bromide (CTAB), sodium hydroxide (NaOH), formic acid, sulfuric acid, and anhydrous ethanol were obtained from Sinopharm Chemical Reagent Co. Ltd (Shanghai, China). A 5 wt% Nafion solution (perfluorinated ion-exchange resin, a mixture of lower aliphatic alcohols and water) was purchased from Sigma-Aldrich. All the chemicals reagents are of analytical grade in this experiment. The water throughout the experiment was triple-distilled water.

2.2. Synthesis of nanocatalysts in DESs

The choline chloride-urea DESs were prepared according to the method previously reported [26−28]. Choline chloride and urea were recrystallized from absolute ethanol and triple-distilled water, respectively, filtered and dried under vacuum prior to use. 140 g of choline chloride and 120 g of urea were stirred together at 80 °C until a homogeneous and colorless liquid was formed. The DESs, once formulated, were kept in a vacuum at 80 °C prior to use. 3D Pd-FNNs were prepared according to the following process: 1 mL $PdCl_2$/DESs (0.0564 $mol \cdot L^{-1}$) was pipetted into 10 mL DESs with vigorous stirring, and followed by an additional 3 mL of NaOH/DESs (0.1 $mol \cdot L^{-1}$) solution with continuous stirring for 20 min. Subsequently, 5 mL CTAB/DESs (0.0165 $mol \cdot L^{-1}$)

solution was slowly dropwise added to the above solution, followed by continuous stirring for 30 min. Finally, 3 mL freshly prepared ascorbic acid (0.2 $mol \cdot L^{-1}$) was slowly added into the above system and homogeneously mixed by continuous stirring. After solvothermal treatment at 150 °C for 8 h in a 30-mL autoclave, the resulting black solid was collected by centrifugation and washed repeatedly with triple-distilled water, absolute ethanol, and cyclohexane to remove possible residual ions and polymer in the final product. The as-prepared samples were then dried in a vacuum oven at 60 °C for 12 h. As a comparison, the sample in water medium (Pd-Water) was also prepared using the similar procedure as described above.

2.3. Physical characterizations

A Holland PHILPS Quanta 200FEG FEI field emission environmental scanning electron microscope (SEM) equipped with an energy-dispersive X-ray spectroscopic analyzer. Energy dispersion X-ray spectra analysis (EDX) was used to analyze the chemical composition of nanocatalysts. The morphological analysis of the as-prepared products was done by high-resolution transmission electron microscope (HRTEM, JEOL JEM-2100) with an accelerating voltage of 200 kV. The crystalline structures were examined by powder X-ray diffraction (XRD) on an X-ray diffractometer (Rigaku D/MAX 2500 v/pc, Japan) using a Cu K_α radiation source ($\lambda = 1.5406$ Å). The surface information of the as-prepared nanocatalysts was obtained by X-ray photoelectron spectroscopy (XPS), which was performed on a Thermo Scientific ESCALAB 250Xi system using Al K_α radiation.

2.4. Electrochemical characterizations

All electrochemical experiments were conducted with a CHI 660D electrochemical workstation. A saturated calomel electrode (SCE) was used as the reference electrode, and a piece of platinum foil (1 cm^2) was served as the counter electrode. The working electrode was a modified glassy carbon electrode (GCE, 5 mm in diameter). For preparation of the modified electrodes, 1.5 mg of dried catalyst was dispersed ultrasonically into 3 mL of anhydrous ethanol and 50 μL Nafion solution (5 wt%), sonicated for 30 min to obtain a homogeneous catalyst suspension. Next, 15 μL of the electrocatalyst suspension was drop-cast onto the mirror-polished GCE surface and allowed to evaporate at room temperature before use.

All electrolytes were purged with N_2 for 15 min before each electrochemical experiment, and a flux of N_2 was kept over the solution throughout the measurements to prevent the interference from atmospheric oxygen. Electrocatalytic performance of all catalysts toward formic acid oxidation testing was investigated in 0.5 $mol \cdot L^{-1}$ H_2SO_4 and 1 $mol \cdot L^{-1}$ HCOOH solutions at a scan rate of 50 $mV \cdot s^{-1}$. For CO stripping measurements, pure CO was bubbled into 0.5 $mol \cdot L^{-1}$ H_2SO_4 for 10 min to allow saturated adsorption of CO onto the catalyst while holding the potential sweep between −0.2 and 0 V. Then the electrolyte was purged with N_2 for 20 min to remove the dissolved CO in the electrolyte before the measurements were taken. Electrochemical active surface area (ECSA) can be calculated from CO adsorption/desorption curves, which assumes CO adsorption as a monolayer adsorption. All electrochemical measurements were performed at around 25 °C.

3. Results and discussion

3.1. Characterizations of Pd nanostructures

The morphology and microstructure of the as-prepared sample under the optimal experimental conditions were characterized in detail by SEM and TEM, as shown in Fig. 1. The low-magnification SEM images (Fig. 1a−d) distinctly manifest that the flower-like units are assembled into network nanostructure with highly active area. Furthermore, a close look at the high-magnification SEM image in the inset of Fig. 1b reveals that the flower-like units are indeed composed of nanosheets and nanospheres subunits. Fig. 1e and f displays typical TEM images of the Pd-FNNs, further verifying the successful synthesis of 3D flower-like Pd network nanostructures, where the nanosheet subunits can be clearly seen on the surface of the flower-like structure units. Pd nanosheets are considered to be an efficient nanomaterial due to their large surface area-to-volume ratio and abundant exposed (100) crystal faces [29]. Therefore, it can be predicted that the Pd-FNNs catalyst significantly increase the ECSA and enhance its electro-catalytic performance. The inset of Fig. 1f shows a typical SAED image of the nanosheets subunit, demonstrating the well-defined polycrystalline structure. The formation process of Pd-FNNs might be as follows: part of the precursors rapidly formed spherical primary nanoparticles with a reducing agent; the other part of the precursors was converted into nanosheet structures due to the adsorption of surfactants; thereafter, the above two nanostructures would rapidly reorganize into flower-like units, and then self-assemble into network nanostructures with abundance of grain boundaries. This is similar to

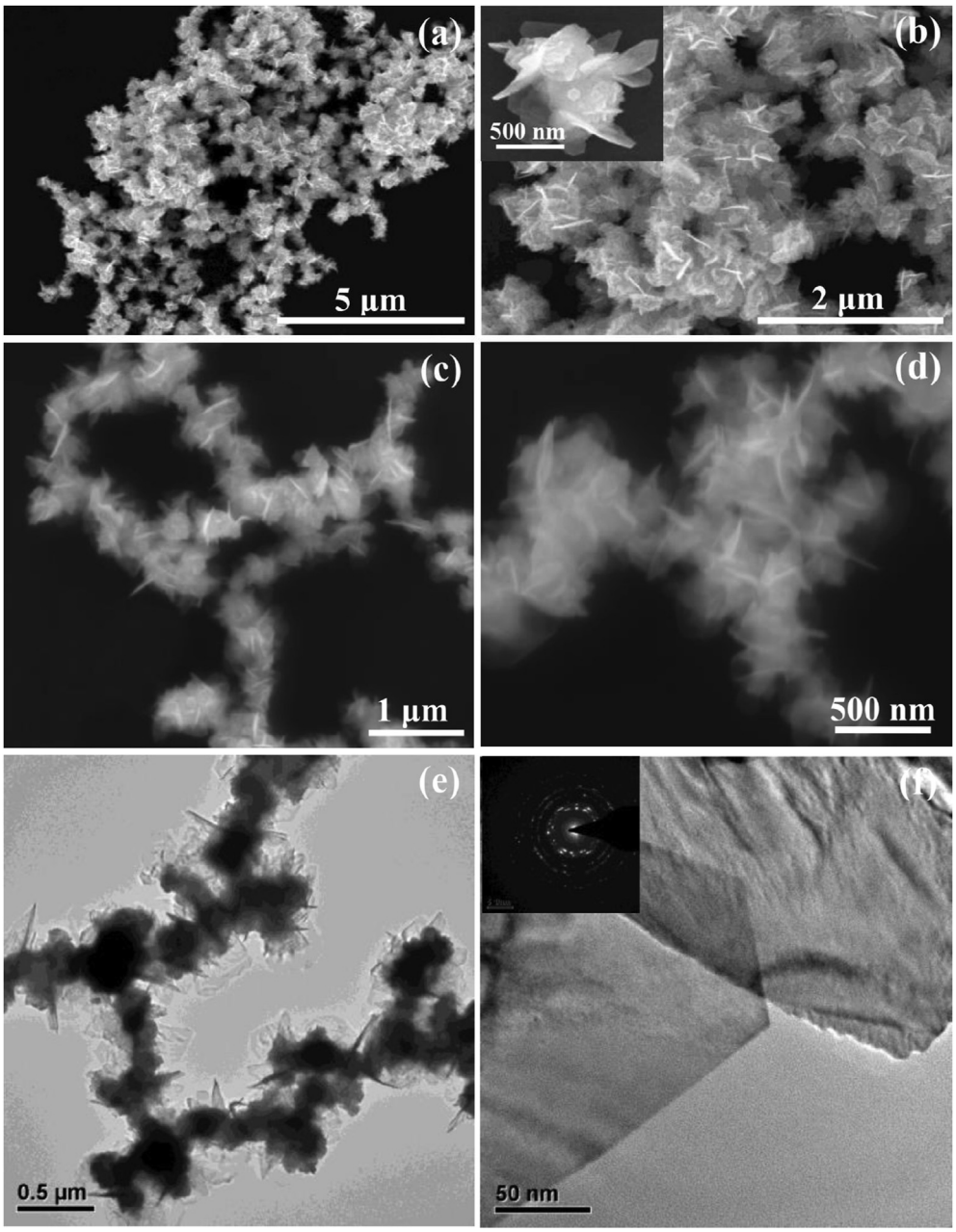

Fig. 1. SEM images (a, b, c and d) and TEM images (e and f) of Pd-FNNs. The insets in (b) and (f) are the high-magnification SEM and SAED images, respectively.

the formation process of branched and multipodal structures, namely, "seeded growth" and "self-organization" mechanisms [30].

Fig. 2a shows the XRD pattern of 3D flower-like Pd network nanostructures. The strong characteristic diffraction peaks located at $2\theta = 39.9^\circ$, 46.3°, 67.9°, 81.8°, and 86.6° are attributed to Pd(111), Pd(200), Pd(220), Pd(311), and Pd(222) crystal facets (JCPDS card, PDF # 87-0643), respectively, which can be indexed as face centered cubic (fcc) crystal structure. In addition, the XRD result confirms the formation of pure Pd powder with high crystallinity, which is consistent with the results of SAED. The EDX image of Pd-FNNs is shown in Fig. 2b. The signals of C, O, and Pd elements can be seen from the EDX spectrum, demonstrating the successful preparation of Pd nanostructures. And the signal of C may be caused by the conductive tape as a substrate.

The elemental composition and chemical valence state of Pd-FNNs surface were monitored by XPS. The signals of O and Pd elements can be obtained from Fig. 2c, which is consistent with the result of EDX. The signal peaks of Pd 4p (51.4 eV), Pd 3 d (335.6 eV), O 1s (532.6 eV), Pd 3p (559.5 eV), and Pd 3s (670.5 eV) further confirmed the successful

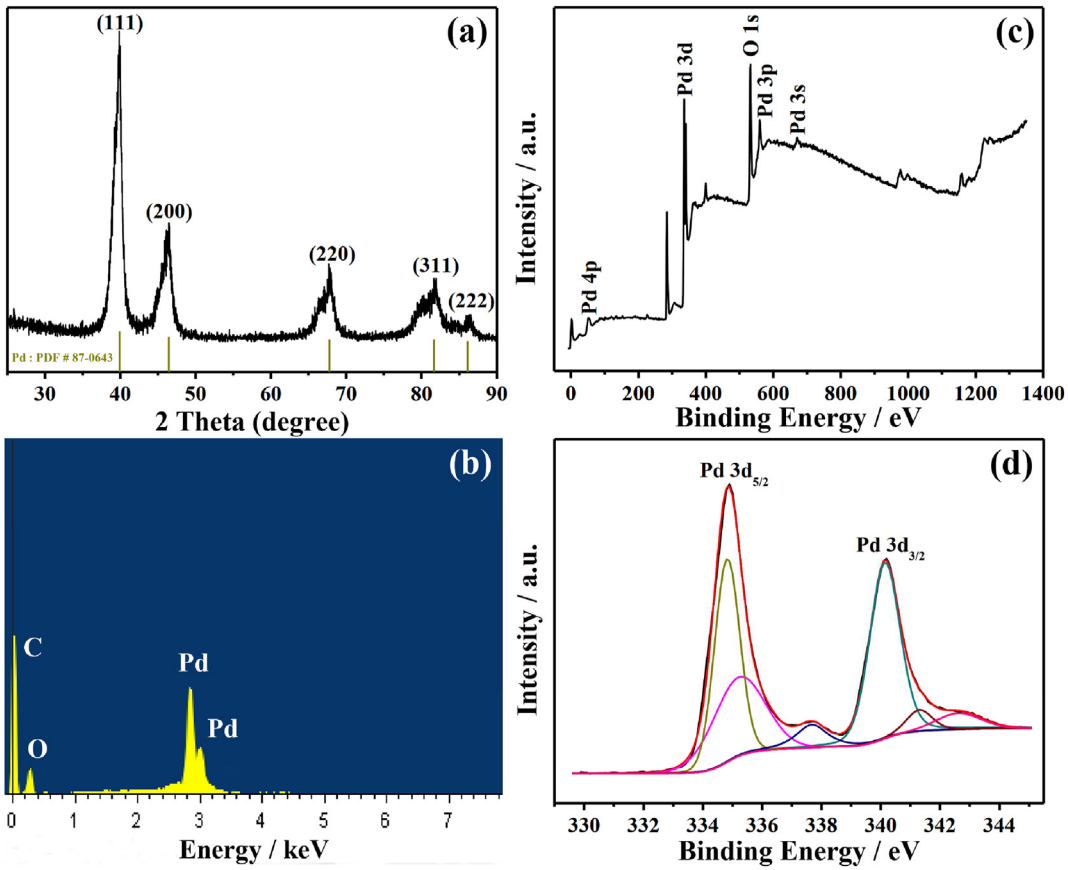

Fig. 2. XRD (a) and EDX (b) patterns of Pd-FNNs, XPS survey spectrum of Pd-FNNs (c) and high-resolution spectra of Pd 3 d (d).

preparation of Pd nanostructures. Fig. 2d is the high-resolution spectra of Pd 3 d. Three pairs of deconvoluted peaks indicate the existence of three different Pd oxidation states on the catalytic surface. A double strong peak centered at 334.8 eV and 340.2 eV corresponds to Pd $3d_{5/2}$ and Pd $3d_{3/2}$ peaks of metallic state Pd, respectively. The Pd $3d_{5/2}$ (335.3 eV) and Pd $3d_{3/2}$ (341.3 eV) exist in the form of PdO. Moreover, the other double peak of Pd $3d_{5/2}$ (337.7 eV) and Pd $3d_{3/2}$ (342.7 eV) belong to Pd (IV) species. The existence of 63.3% Pd (0) species in Pd-FNNs is obtained by calculating the relative peak areas, indicating that $PdCl_2$ was efficiently reduced by ascorbic acid. In particular, the metal state of Pd is the main oxidation sites of formic acid molecules through the non-CO pathway [31], so it can be speculated that the Pd-FNNs have better FAOR performance.

3.2. Study on the formation mechanism of Pd-FNNs

In theory, the formation of nanostructures includes two processes, nucleation and growth, which is powerfully influenced by external conditions and intrinsic crystal structure. External conditions are some of kinetic and thermodynamic factors, including reducing agent, reaction temperature, reaction time, and surfactant, etc. Further growth of primary nuclei can be obtained by consumption of reactants or metastable particles. Nanosheet structures have high surface energy, and are easy to be aggregated during the early stage of the growth process. Therefore, fine-tuning of the reaction conditions is required to prepare 3D flower-like Pd network nanostructures with nanosheet structural units. Here, DESs and CTAB (a negatively charged electrolyte stabilizer) can be used as a soft template for the successful synthesis of Pd-FNNs.

In order to investigate the influence of external conditions on the nanostructure growth process, the alkalinity of reaction medium, the reaction temperature, and the amount of surfactant were studied. Firstly, the different volumes of NaOH/DESs (0.1 $mol \cdot L^{-1}$) solutions were added into reaction system. Fig. S1 is the SEM images of the as-prepared samples by adding 1, 5, 7, 9 mL of NaOH/DESs. By comparing Fig. 1 and Fig. S1, it can be found that the nanosheet units were generated in the case of a weak alkaline medium, where the best nanostructure was obtained by adding 3 mL of NaOH/DESs (Fig. 1a). With the increase of

alkalinity, the nanosheets gradually curled into spherical particles, and the connections between particles became tighter. When 9 mL of NaOH/DESs was added into the reaction system, the rod-like structures with larger sizes were formed (Fig. S1d). The results illustrate that the growth of Pd nanostructures is controlled by the alkalinity of the reaction medium, which may be due to the decrease in reducing ability of AA with increasing pH [32].

Reaction temperature can also directly affect the dynamic process of the nanostructure growth. Adjusting the reaction temperature is crucial for controlling the reaction rate and the assembly of nuclei. Several samples were prepared separately at 130, 150, 170 and 190 °C, and their representative SEM images are shown in Fig. S2. When the temperature was lower (130 °C, Fig. S2a), the sample was mainly composed of a layered packing structure. And the 3D flower-like Pd network nanostructures were obtained when the temperature was raised to 150 °C (Fig. S2b). Further heating up to 170 °C, in order to reduce the surface energy and exist in a stable state, the nanosheets curled into an obvious layered structure (Fig. S2c). When the temperature was raised to 190 °C, the samples were transformed into nano-dendritic network structures (Fig. S2d).

The presence of CTAB plays an important role in the anisotropic growth and generation of Pd nanosheets [33]. To uncover the effect of CTAB/DESs concentration on the morphology of final products, we acquired the products by adding different amounts of CTAB/DESs solution. As can be seen from Fig. S3, in the range of 7 mL dosage, we obtained the products with different structures, suggesting that CTAB plays an important role in the shape-controlled synthesis of Pd-FNNs. When no CTAB/DESs solution was added to the reaction system, the morphology of coral-like Pd network nanostructures (Pd-CNNs) composed of larger size spherical units was generated (Fig. S3a). When 1 mL CTAB/DESs solution was added, the Pd-CNNs were still formed, but the size of spherical units decreased significantly (Fig. S3b). Continuing to increase the amount of CTAB/DESs solution up to 3 mL, the Pd-CNNs were damaged and began to appear obvious nanosheets structure (Fig. S3c). If the dosage of CTAB/DESs solution was further increased to 5 mL, the morphology of perfect Pd-FNNs appeared (Fig. 1a). However, when the amount of CTAB/DESs solution was larger (7 mL), the number of nanosheets decreased and a clear aggregation phenomenon was observed (Fig. S3d).

3.3. Evaluation of electrocatalytic performance

Fig. 3a shows the cyclic voltammograms (CV) of Pd nanostructures synthesized in DESs or water, as well as commercial Pd black in N_2-saturated 0.5 mol·L^{-1} H_2SO_4 aqueous solution. The shape of the curves is consistent with the results reported in literature, including the hydrogen absorption/desorption peaks between −0.2 and 0.1 V, and the oxidation/reduction peaks of Pd. In contrast, the reduction peak area of Pd-FNNs is the largest at ca. 0.5 V, so it may have more active sites and larger electrochemically active area. For commercial Pd black, the peak near −0.10 V is associated with the hydrogen adsorption on {110} step sites, while the peak around −0.03 V corresponds to the hydrogen adsorption on {100} terrace sites [34−36]. For the other three samples, only the signal of {100} plane appeared on the CV curves. Among three low-index facets, the Pd(100) facet has been reported to exhibit the highest FAOR performance [37−39]. Therefore, the abundant grain boundaries of Pd-FNNs can provide sufficient active sites, and efficiently promote the direct conversion of formic acid molecules to CO_2 product.

FAOR is used as a model reaction to evaluate the electrocatalytic activities of the as-prepared Pd nanostructures, Fig. 3b is the cyclic voltammograms of Pd-FNNs, Pd-CNNs, Pd-Water, and commercial Pd black in 1.0 mol·L^{-1} HCOOH +0.5 mol·L^{-1} H_2SO_4 solutions. All the four catalysts have characteristic peaks of irreversible cyclic voltammetry. During the forward sweep, the anodic peaks near 0.3 V are attributed to the oxidation of formic acid through the direct pathway; with the increase of the potential, in the high-potential region of >0.6 V, the Pd on the catalyst surface is gradually oxidized, inhibiting the adsorption of reactant molecules and reducing the FAOR activity. Thus, this process involves a change of rate-determining step: from the adsorption of oxygen-containing species to the adsorption of reaction intermediates (e.g., HCOO* or COOH*) [7,40]. During the negative sweep process, the oxidized-Pd is reduced to bare Pd active sites, and the subsequent sharply increased current density is attributed to the electrocatalytic oxidation of formic acid on Pd catalysts. The Pd-FNNs appears a main oxidation peak in the vicinity of 0.28 V during the positive sweeping process, and another positive sweeping peak is hardly observed, illustrating the FAOR mainly go through the direct dehydrogenation pathway, and the catalyst is rarely poisoned by CO intermediates. That is, formic acid molecules are adsorbed on the catalyst surface form COOH* or HCOO* intermediates via

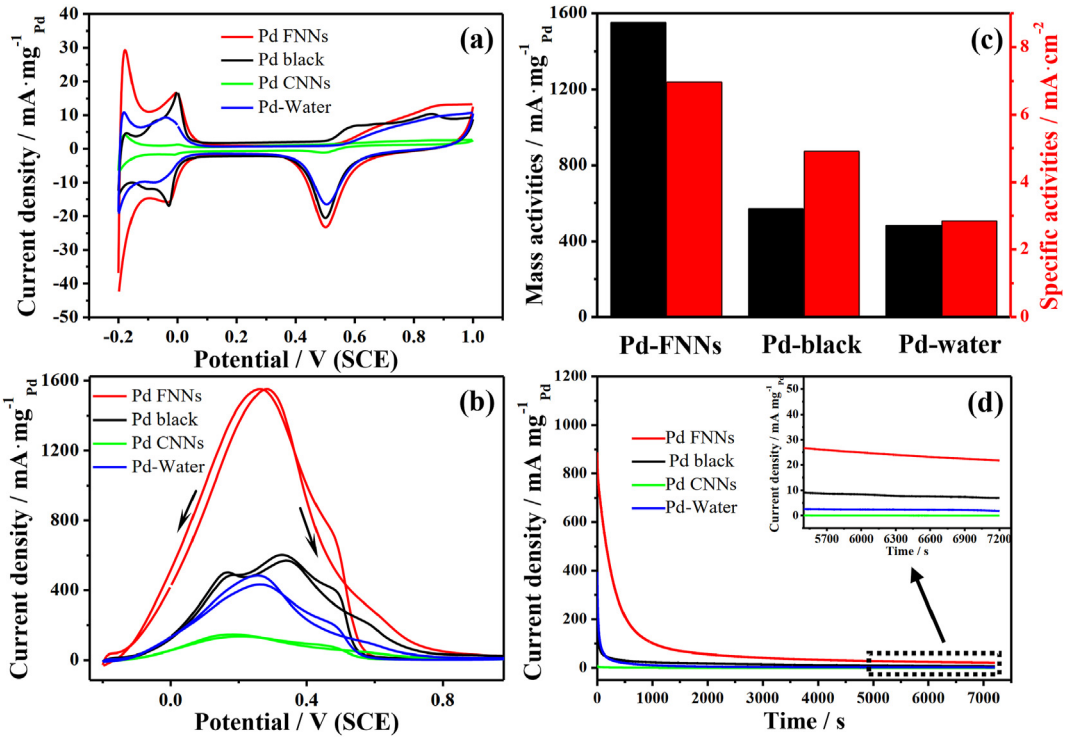

Fig. 3. Cyclic voltammograms of Pd-FNNs, Pd-CNNs, Pd-Water, and commercial Pd black in 0.5 mol·L^{-1} H_2SO_4 (a) and 1.0 mol·L^{-1} HCOOH + 0.5 mol·L^{-1} H_2SO_4 (b) solutions at a scan rate of 50 mV·s^{-1}. Comparison plots of mass activities and specific activities (c). Current-time curves of HCOOH oxidation on four catalysts in 1.0 mol·L^{-1} HCOOH +0.5 mol·L^{-1} H_2SO_4 solution, at a potential of 0.1 V (d).

the first dehydrogenation step, and then continue to remove another hydrogen atom to generate CO_2 [7,41,42]. In addition, the Pd-FNNs has the lowest onset potential of formic acid oxidation compared with the Pd-CNNs, Pd-Water, and commercial Pd black (Fig. S4), indicating that the Pd-FNNs is mostly prone to oxidizing formic acid molecules. This is due to the fact that the connected network structure facilitates the electron transfer and improves the oxidation of formic acid. Although the Pd-CNNs also possess the network structure, the larger diameter of spherical units severely hinders the FAOR, namely, it shows the highest onset oxide potential and the lowest mass activity (134.7 mA·mg$^{-1}_{Pd}$). The mass activity of Pd-FNNs was 1551.8 mA·mg$^{-1}_{Pd}$ for FAOR, which is 2.7 and 3.2 times higher than those of the commercial Pd black (570.1 mA·mg$^{-1}_{Pd}$) and Pd-water (484.2 mA·mg$^{-1}_{Pd}$), respectively (Fig. 3c). This demonstrates that the Pd-FNNs have a significant enhancing effect on the electrocatalytic oxidation of formic acid, which is attributed to the synergistic effect of special network nanostructure, abundant boundary sites, and (100) crystal planes.

The long-term electrocatalytic activity and stability of the synthesized Pd nanostructures and commercial Pd black toward the FAOR were further characterized by chronoamperometric tests at 0.1 V potential (Fig. 3d). All the four catalysts had high current densities in the initial stage, which is caused by electric double layer charging and abundant active sites for the catalyst. However, the current density rapidly decreased at 300 s, due to the strong adsorption of reaction intermediates on the catalyst surface during the FAOR process. Nevertheless, the Pd-FNNs had the highest current density in the whole process of FAOR. Moreover, the steady-state current density of Pd-FNNs is 3.1 and 12.3 times higher than those of commercial Pd black and Pd-water, respectively, further confirming its high electrocatalytic activity and long-term stability. The Pd-CNNs catalyst is almost inactive in the end. The enhanced stability of Pd-FNNs is also mainly due to the special network nanostructure and synergistic effect.

The resistance of catalyst to CO poisoning is one of the important indicators to measure the performance of catalyst, so the CO electro-oxidizing behavior was examined by CO stripping voltammetric experiments. Fig. 4 shows the CO stripping voltammetric curves of Pd-FNNs (a), commercial Pd black (b), Pd-CNNs (c), and Pd-water (d) in 0.5 mol·L^{-1} H_2SO_4 solution at a scan rate of 50 mV·s^{-1}. As can be seen from the graphs, the adsorption/desorption peaks of hydrogen are completely suppressed before oxidization of CO_{ads} (the red curve). Then, the adsorption/desorption peaks of hydrogen occur again when the CO_{ads} is

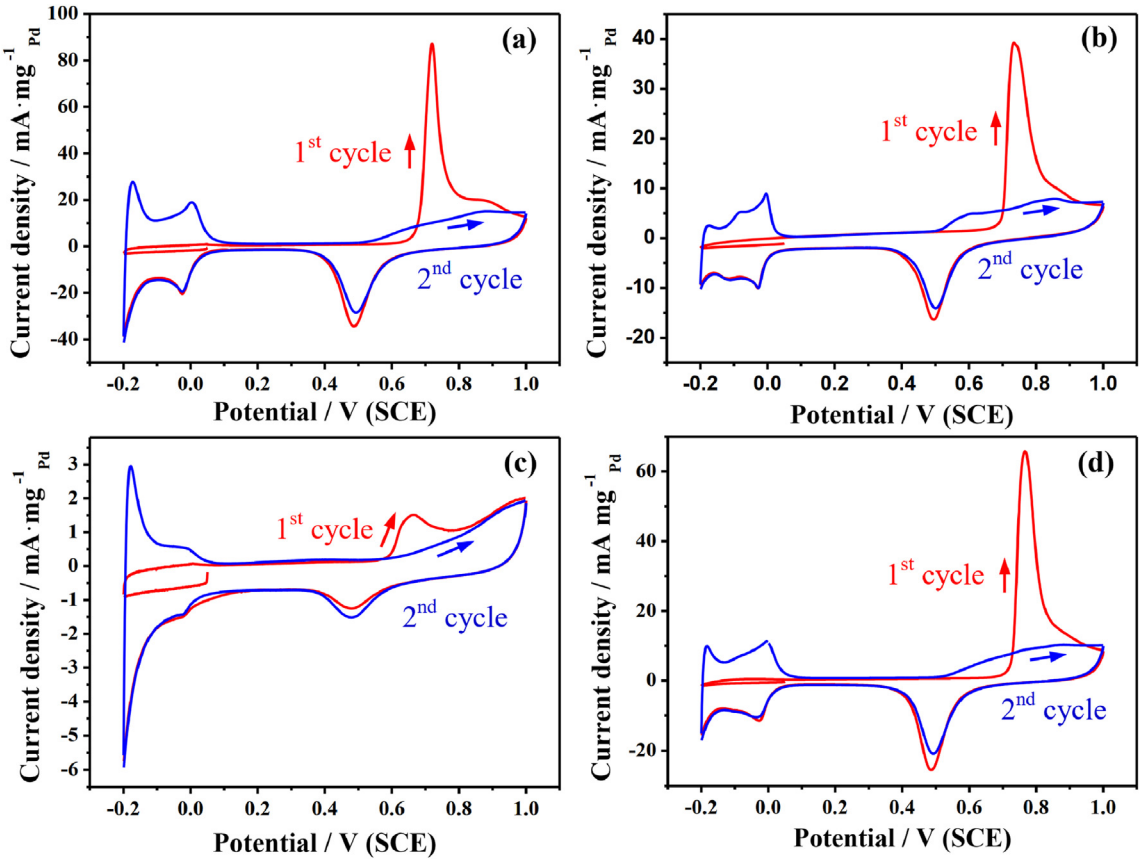

Fig. 4. CO stripping voltammograms of Pd-FNNs (a), commercial Pd black (b), Pd-CNNs (c), and Pd-Water (d) catalysts in 0.5 mol·L^{-1} H_2SO_4 at a scan rate of 50 mV·s^{-1}.

completely oxidized (the blue curve), indicating that CO has been saturated on the surface of Pd catalyst. The surface CO oxidation onset potential of Pd-FNNs was 0.54 V, which is lower than those of Pd-CNNs (0.57 V), commercial Pd black (0.60 V), and Pd-water (0.62 V), indicating that the Pd-FNNs has better resistance ability to CO poisoning. Moreover, the CO oxidation peak potentials of Pd-FNNs were negatively shifted by 47 and 17 mV compared to Pd-CNNs and commercial Pd black (Fig. S5), respectively. In general, high ECSA represents high electrocatalytic activity. Since the adsorption/desorption process of hydrogen on the Pd surface is accompanied by hydrogen into the Pd lattice, CO oxidation current (Q_{CO}) is generally used to calculate the ECSA of Pd-base catalysts. According to the formula of ECSA = Q_{CO}/420 ($\mu C \cdot cm^{-2}$)/W_{Pd}, the ECSA of Pd-FNNs is 22.3 $m^2 \cdot g_{Pd}^{-1}$, which is higher than those of Pd-water (17.0 $m^2 \cdot g_{Pd}^{-1}$), commercial Pd black (11.6 $m^2 \cdot g_{Pd}^{-1}$), and Pd-CNNs (0.73 $m^2 \cdot g_{Pd}^{-1}$), indicating that the Pd-FNNs catalyst has a larger ECSA and is conducive to the electrocatalytic oxidation of formic acid. From the results of ECSA, the specific activities of the Pd-FNNs, commercial Pd black, and Pd-CNNs catalysts can be calculated to be 6.96, 4.91, and 2.85 mA·cm^{-2} (Fig. 3c), respectively. Compared with some Pd-based FAOR catalysts reported in the literature, this Pd-FNNs catalyst has higher electrocatalytic performance (Table S1).

4. Conclusions

In this work, the Pd-FNNs catalyst was successfully synthesized in DESs by a simple and effective solvent thermal method. XRD, SEM, and TEM results showed that the catalyst displayed the flower-like network polycrystalline structure, and this structure significantly enhanced the ECSA and electro-catalytic performance for FAOR. XPS analysis demonstrated that the Pd mainly existed in the form of metallic state in the Pd-FNNs, accounting for 63.3% of the total. The mass activity and specific activity of Pd-FNNs are 2.7-folds and 1.4-folds higher than those of commercial Pd black, respectively. The superior electrocatalytic performance and anti-CO poisoning ability are mainly attributed to the synergistic effect of the unique network nanostructure and abundant boundary sites. This work provides an avenue for the design and preparation of novel DFAFC anode catalysts.

Acknowledgements

The project was supported by the National Natural Science Foundation of China (22162006), the China Postdoctoral Science Foundation (2021M 691366) and the Natural Science Foundation of Shanxi Province (20210302124473).

References

[1] Zhang S, Xia R, Su Y, Zou Y, Hu C, Yin G, Hensen E JM, Ma X, Lin Y. 2D surface induced self-assemble of Pd nanocrystals into nanostrings for enhanced formic acid electrooxidation[J]. J. Mater. Chem. A, 2020, 8(33): 17128−17135.

[2] Ding J, Liu Z, Liu X R, Liu B, Liu J, Deng Y D, Han X P, Hu W B, Zhong C. Tunable periodically ordered mesoporosity in palladium membranes enables exceptional enhancement of intrinsic electrocatalytic activity for formic acid oxidation[J]. Angew. Chem. Int. Ed., 2020, 59(13): 5092−5101.

[3] Huang L, Zhan M, Wang Y C, Lin Y F, Liu S, Yuan T, Yang H, Sun S G. Syntheses of carbon paper supported high-index faceted Pt nanoparticles and their performance in direct formic acid fuel cells[J]. J. Electrochem., 2016, 22(2): 123−128.

[4] Jiang M C, Meng X M, Zhang W L, Huang H W, Wang F Q, Wang S, Ouyang Y R, Yuan W Y, Zhang L Y. Facile synthesis of heterophase sponge-like Pd toward enhanced formic acid oxidation[J]. Electrochem. Commun., 2021, 126(1): 107004−107008.

[5] Lv F, Huang B L, Feng J R, Zhang W Y, Wang K, Li N, Zhou J H, Zhou P, Yang W X, Du Y P, Su D, Guo S J. A highly efficient atomically thin curved PdIr bimetallene electrocatalyst[J]. Natl. Sci. Rev., 2021, 8(9): 1−11.

[6] Zheng J Z, Zeng H J, Tan C H, Zhang T M, Zhao B, Guo W, Wang H B, Sun Y H, Jiang L. Coral-like PdCu alloy nanoparticles act as stable electrocatalysts for highly efficient formic acid oxidation[J]. ACS Sustainable Chem. Eng., 2019, 7(18): 15354−15360.

[7] Zhang J M, Shen L F, Jiang Y X, Sun S G. Random alloy and intermetallic nanocatalysts in fuel cell reactions[J]. Nanoscale, 2020, 12(38): 19557−19581.

[8] Perales-Rondon J V, Ferre-Vilaplana A, Feliu J M, Herrero E. Oxidation mechanism of formic acid on the bismuth adatom-modified Pt(111) surface[J]. J. Am. Chem. Soc., 2014, 136(38): 13110−13113.

[9] Zhang J M, Wang R X, Nong R J, Li Y, Zhang X J, Zhang P Y, Fan Y J. Hydrogen co-reduction synthesis of PdPtNi alloy nanoparticles on carbon nanotubes as enhanced catalyst for formic acid electrooxidation[J]. Int. J. Hydrogen Energy, 2017, 42(10): 7226−7234.

[10] Shen T, Zhang J J, Chen K, Deng S F, Wang D L. Recent progress of palladium-based electrocatalysts for the formic acid oxidation reaction[J]. Energ. Fuel., 2020, 34(8): 9137−9153.

[11] Yan Y C, Li X, Tang M, Zhong H, Huang J B, Bian T, Jiang Y, Han Y, Zhang H, Yang D R. Tailoring the edge sites of 2D Pd nanostructures with different fractal dimensions for enhanced electrocatalytic performance[J]. Adv. Sci., 2018, 5(8): 1800430−1800436.

[12] Ren M J, Zou L L, Chen J, Yuan T, Huang Q H, Zhang H F, Yang H, Feng S L. Electrocatalytic oxidation of formic acid on Pd/Ni heterostructured catalyst[J]. J. Electrochem., 2012, 18(6): 515−520.

[13] Xiao C, Tian N, Zhou Z Y, Sun S G. Electrochemical preparations and applications of nano-catalysts with high-index facets[J]. J. Electrochem., 2020, 26(1): 61−72.

[14] Zhang L Y, Ouyang Y, Wang S, Gong Y, Jiang M, Yuan W, Li C M. Ultrafast synthesis of uniform 4−5 atoms-thin layered tremella-like Pd nanostructure with extremely large electrochemically active surface area for formic acid oxidation[J]. J. Power Sources, 2020, 447(1): 227248−227254.

[15] Poerwoprajitno A R, Gloag L, Cheong S, Gooding J J, Tilley R D. Synthesis of low- and high-index faceted metal (Pt, Pd, Ru, Ir, Rh) nanoparticles for improved activity and stability in electrocatalysis[J]. Nanoscale, 2019, 11(9): 18995−19011.

[16] Xu B Y, Zhang Y, Li L G, Shao Q, Huang X Q. Recent progress in low-dimensional palladium-based nanostructures for electrocatalysis and beyond[J]. Coordin. Chem. Rev., 2022, 459(5): 214388−214419.

[17] Xiao C, Lu B A, Xue P, Tian N, Zhou Z Y, Lin X, Lin W F, Sun S G. High-index-facet- and high-surface-energy nanocrystals of metals and metal oxides as highly efficient catalysts[J]. Joule, 2020, 4(12): 2562−2598.

[18] Gong Y, Liu X, Gong Y, Wu D, Xu B, Bi L, Zhang L Y, Zhao X S. Synthesis of defect-rich palladium-tin alloy nanochain networks for formic acid oxidation[J]. J. Colloid Interf. Sci., 2018, 530(11): 189−195.

[19] Xu Y, Xu R, Cui J H, Liu Y, Zhang B. One-step synthesis of three-dimensional Pd polyhedron networks with enhanced electrocatalytic performance[J]. Chem. Commun., 2012, 48(32): 3881−3883.

[20] Yuan T, Chen H Y, Ma X, Feng J J, Yuan P X, Wang A J. Simple synthesis of self-supported hierarchical AuPd alloyed nanowire networks for boosting electrocatalytic activity toward formic acid oxidation[J]. J. Colloid Interf. Sci., 2018, 513(3): 324−330.

[21] Zhang X F, Chen Y, Zhang L, Wang A J, Wu L J, Wang Z G, Feng J J. Poly-L-lysine mediated synthesis of palladium nanochain networks and nanodendrites as highly efficient electrocatalysts for formic acid oxidation and hydrogen evolution[J]. J. Colloid Interf. Sci., 2018, 516(4): 325−331.

[22] Cui X, Xiao P, Wang J, Zhou M, Guo W L, Yang Y, He Y J, Wang Z W, Yang Y K, Zhang Y H, Lin Z Q. Highly branched metal alloy networks with superior activities for the methanol oxidation reaction[J]. Angew. Chem. Int. Ed., 2017, 56(16): 4488−4493.

[23] Zhang Q B, Hua Y X. Electrochemical synthesis of copper nanoparticles using cuprous oxide as a precursor in choline chloride-urea deep eutectic solvent: nucleation and growth mechanism[J]. Phys. Chem. Chem. Phys., 2014, 16(48): 27088−27095.

[24] Kumar-Krishnan S, Prokhorov E, Arias de Fuentes O, Ramõrez M, Bogdanchikova N, Sanchez I C, Mota-Morales J D, Luna-Barcenas G. Temperature-induced Au nanostructure synthesis in a nonaqueous deep-eutectic solvent for high performance electrocatalysis[J]. J. Mater. Chem., 2015, 3(31): 15869−15875.

[25] Wagle D V, Zhao H, Baker G A. Deep eutectic solvents: sustainable media for nanoscale and functional materials [J]. Acc. Chem. Res., 2014, 47(8): 2299−2308.

[26] Wei L, Fan Y J, Tian N, Zhou Z Y, Zhao X Q, Mao B W, Sun S G. Electrochemically shape-controlled synthesis in deep eutectic solvents—a new route to prepare Pt nanocrystals enclosed by high-index facets with high catalytic activity[J]. J. Phys. Chem. C, 2012, 116(2): 2040−2044.

[27] Wei L, Fan Y J, Wang H H, Tian N, Zhou Z Y, Sun S G. Electrochemically shape-controlled synthesis in deep eutectic solvents of Pt nanoflowers with enhanced activity for ethanol oxidation[J]. Electrochim. Acta, 2012, 76(8): 468−474.

[28] Wei L, Xu C D, Huang L, Zhou Z Y, Chen S P, Sun S G. Electrochemically shape-controlled synthesis of Pd concave

disdyakis triacontahedra in deep eutectic solvent[J]. J. Phys. Chem. C, 2016, 120(29): 15569−15577.
[29] Yin X, Chen Q Y, Tian P, Zhang P, Zhang Z Y, Voyles P M, Wang X D. Ionic layer epitaxy of nanometer-thick palladium nanosheets with enhanced electrocatalytic properties [J]. Chem. Mater., 2018, 30(10): 3308−3314.
[30] Jana R, Subbarao U, Peter S C. Ultrafast synthesis of flower-like ordered Pd_3Pb nanocrystals with superior electrocatalytic activities towards oxidation of formic acid and ethanol[J]. J. Power Sources, 2016, 301(1): 160−169.
[31] Shan J F, Lei Z, Wu W, Tan Y Y, Cheng N C, Sun X L. Highly active and durable ultrasmall Pd nanocatalyst encapsulated in ultrathin silica layers by selective deposition for formic acid oxidation[J]. ACS Appl. Mater. Interfaces, 2019, 11(46): 43130−43137.
[32] Huang H W, Ruditskiy A, Choi S I, Zhang L, Liu J Y, Ye Z Z, Xia Y N. One-pot synthesis of penta-twinned palladium nanowires and their enhanced electrocatalytic properties [J]. ACS Appl. Mater. Interfaces, 2017, 9(36): 31203−31212.
[33] Saravani H, Farsadrooh M, Mollashahi M S, Hajnajafi M, Douk A S. Two-dimensional engineering of Pd nanosheets as advanced electrocatalysts toward formic acid oxidation [J]. Int. J. Hydrogen Energ., 2020, 45(41): 21232−21240.
[34] Lou Y Y, Xiao C, Fang J, Sheng T, Ji L, Zheng Q, Xu B B, Tian N, Sun S G. The high activity of step sites on Pd nanocatalysts in electrocatalytic dechlorination[J]. Phys. Chem. Chem. Phys., 2022, 24(6): 3896−3904.
[35] Yu N F, Tian N, Zhou Z Y, Sheng T, Lin W F, Ye J Y, Liu S, Ma H B, Sun S G. Pd nanocrystals with continuously tunable high-index facets as a model nanocatalyst[J]. ACS Catal., 2019, 9(4): 3144−3152.
[36] Xiao C, Tian N, Li W Z, Qu X M, Du J H, Lu B A, Xu B B, Zhou Z Y, Sun S G. Shape transformations of Pt nanocrystals enclosed with high-index facets and low-index facets[J]. CrystEngComm, 2021, 23(38): 6655−6660.
[37] Shen T, Chen S J, Zeng R, Gong M X, Zhao T H, Lu Y, Liu X P, Xiao D D, Yang Y, Hu J P, Wang D L, Xin H L, Abruna H D. Tailoring the antipoisoning performance of Pd for formic acid electrooxidation via an ordered PdBi intermetallic[J]. ACS Catal., 2020, 10(17): 9977−9985.
[38] Shi Y F, Lyu Z H, Cao Z M, Xie M H, Xia Y N. How to remove the capping agent from Pd nanocubes without destructing their surface structure for the maximization of catalytic activity?[J]. Angew. Chem. Int. Ed., 2020, 59(43): 19129−19135.
[39] Rettenmaier C, Aran-Ais R M, Timoshenko J, Rizo R, Jeon H S, Kuhl S, Chee S W, Bergmann A, Cuenya B R. Enhanced formic acid oxidation over SnO_2-decorated Pd nanocubes[J]. ACS Catal., 2020, 10(1): 14540−14551.
[40] Mondal S, Raj C R. Electrochemical dealloying-assisted surface-engineered Pd-based bifunctional electrocatalyst for formic acid oxidation and oxygen reduction[J]. ACS Appl. Mater. Interfaces, 2019, 11(15): 14110−14119.
[41] Wang W C, He T O, Yang X L, Liu Y M, Wang C Q, Li J, Xiao A D, Zhang K, Shi X T, Jin M S. General synthesis of amorphous PdM (M = Cu, Fe, Co, Ni) alloy nanowires for boosting HCOOH dehydrogenation[J]. Nano Lett., 2021, 21(8): 3458−3464.
[42] Shi W, Park A H, Xu S, Yoo P J, Kwon Y U. Continuous and conformal thin TiO_2-coating on carbon support makes Pd nanoparticles highly efficient and durable electrocatalyst[J]. Appl. Catal. B-Environ., 2021, 284(5): 119715−119724.

低共熔溶剂辅助合成新型的网状纳米结构用于加速甲酸电氧化

张俊明[a,b,c,*]，张小杰[a,b]，陈　瑶[a]，房英健[a]，樊友军[b,*]，贾建峰[a,*]
[a] 山西师范大学化学与材料科学学院，磁性分子与磁信息材料教育部重点实验室，山西 太原 030031
[b] 广西师范大学化学与药学学院，广西低碳能源材料重点实验室，广西 桂林 541004
[c] 昆山良品丝印器材有限公司，江苏 昆山 215300

摘要

低共熔溶剂（DESs）是一种用于可控合成金属纳米结构的溶剂。在氯化胆碱-尿素 DESs 中，使用抗坏血酸作为还原剂可以制备由交错的纳米片和纳米球组成的花状 Pd 纳米颗粒，并且其自发地转化为三维网络纳米结构。此纳米网状结构的形成机制也有系统的研究，其中，DESs 作为溶剂和软模板用于形成 3D 花状钯网络纳米结构（Pd-FNNs），CTAB 和 NaOH 的用量在 Pd-FNNs 的各向异性生长和生成中起着至关重要的作用。Pd 较低的电催化性能是阻碍燃料电池商业化应用的主要挑战之一。然而，具有较低表面能和丰富晶界的 3D Pd-FNNs 对甲酸氧化反应表现出增强的电催化活性和稳定性，其质量活性和本征活性分别是商业 Pd 黑催化剂的 2.7 和 1.4 倍。因此，此策略为合成独特的 Pd 基纳米结构提供了一种可行的路径。

关键词：低共熔溶剂；钯；网络纳米结构；甲酸；电氧化